Far-infrared absorptivity of UPt_3

P. E. Sulewski and A. J. Sievers
Laboratory of Atomic and Solid State Physics and Materials Science Center, Cornell University, Ithaca, New York 14853-2501

M. B. Maple and M. S. Torikachvili
Department of Physics and Institute for Pure and Applied Physical Sciences, University of California, San Diego, La Jolla, California 92093

J. L. Smith and Z. Fisk
Materials Science and Technology Division, Los Alamos National Laboratory, Los Alamos, New Mexico 87545
(Received 15 January 1988)

The absorptivity of the heavy-fermion compound UPt_3 is measured from 2 to 1000 cm^{-1} (0.25–124 meV) at temperatures between 1.2 K and room temperature. Above 50 cm^{-1} (6.2 meV) the absorptivity is relatively temperature independent, while below that frequency the absorptivity is very temperature dependent, in accord with the dc resistivity. By performing a Kramers-Kronig transformation of the data, augmented with recently published results at higher frequencies, the complex conductivity is obtained. The low-temperature conductivity may be characterized by free carriers which undergo frequency-dependent scattering and have a concomitant frequency-dependent mass enhancement, $\lambda(\omega)$, with $\lambda(0)=65$. The data indicate a bare free-carrier plasma frequency of 2.1×10^4 cm^{-1} (2.6 eV). Combining these results with the measured specific heat for UPt_3 gives for the low-frequency effective mass $m^*=240m$, and for the optical band mass $m_b=3.7m$. The carrier density is close to one electron per formula unit. The far-infrared absorptivity measurement indicates that the scattering rate begins to rise with an ω^2 dependence, while the measured dc resistivity has a T^2 dependence at temperatures below 2 K. To account for the far-infrared data, the carrier scattering rate $\Gamma(\omega,T)$ can be written as $\Gamma(\omega,T)\sim\omega^2+(p\pi T)^2$, with an experimental upper limit of $p=1$. This is not consistent with electron-electron scattering, for which $p=2$.

I. INTRODUCTION

Numerous properties of the heavy-fermion (HF) compounds, most notably the low-temperature specific heat and magnetic susceptibility, indicate an enhancement of several hundred in the electron effective mass.[1] Band-structure calculations yield at most a band mass for the conduction electrons of order 10 times the free-electron mass.[2–6] The appearance of such an extraordinary mass in these systems has brought them under intense theoretical and experimental investigation. Among the theoretical concepts is the existence of a characteristic energy scale of the order of a few tens of cm^{-1} (a few meV) (orders of magnitude smaller than the Fermi energy of ordinary metals), analogous to the Kondo temperature for the isolated magnetic impurity case.[7] This energy scale falls in the far-infrared (FIR) spectral region.

Raman scattering,[8,9] inelastic neutron scattering,[10–14] point-contact spectroscopy (PCS),[15] and FIR spectroscopy are techniques capable of probing the electronic structure in the range of tens of cm^{-1} (a few meV). Using Raman scattering, Cooper *et al.*[8,9] observe the predicted phonons for the appropriate space and site groups for UBe_{13}. Comparing Raman spectra of the isostructural compounds[8] MBe_{13} (M=La,Ce,U,Th) reveals an additional electronic scattering in UBe_{13} not observed in the isostructural analogues. Cooper *et al.* attribute this to localized excitations of the $5f$ electrons. While E and M waves couple to the conduction electrons, neutrons couple to the electron spins and so provide a probe of the spin fluctuations. Observations of neutron scattering[14] indicate a predominantly f-electron character of the induced magnetic moment for UPt_3, UBe_{13}, and $CeCu_2Si_2$. Quasielastic lines with widths from 8 cm^{-1} (1 meV) ($CeCu_2Si_2$) (Refs. 10 and 13) to 80 cm^{-1} (10 meV) (UPt_3) (Ref. 11) have also been reported. By measuring the differential resistance as a function of applied voltage across a point contact made to the sample, PCS provides a convolution of the density of states at the Fermi energy and the energy-dependent scattering rate. Moser, Wachter, and Franse[15] interpret their PCS results for UPt_3 as indicating a narrow band of total width 32 cm^{-1} (4 meV) at the Fermi energy. The measurement of the FIR reflectivity of these materials should also provide an excellent probe of the electronic structure of HF systems on the meV scale. Moreover, it now appears likely that HF systems and valence fluctuators (VF's) stem from the same physical interactions.[16] Studies of the reflectivity of the VF compound $CePd_3$ by Pinkerton *et al.*[17] and more recently by Webb, Sievers, and Mihalisin[18] demonstrate the great importance of such reflectivity measurements to understanding the electronic structure of VF materials. Webb, Sievers, and Mihalisin[18] for example were able to separate out contributions to the complex conductivity

for free carriers and bound carriers and identify a frequency-dependent scattering rate which results in a mass enhancement of the free carriers.

Reflectivity measurements are presented in this paper on polycrystalline UPt_3 down to temperatures of 1.2 K and extending in frequency from 2 to 1000 cm^{-1} ($\sim$0.25 to 124 meV). In addition, room-temperature measurements have been made to 5×10^4 cm^{-1} (6 eV). It is shown that the FIR electrodynamic properties of UPt_3 can be characterized most simply by assigning a frequency-dependent scattering rate and a frequency-dependent mass to the charge carriers. The initial rise in the measured scattering rate has an ω^2 dependence with frequency and T^2 with temperature, which presumably arises from the same scattering mechanism as the initial T^2 dependence[19–21] of the dc resistivity; however, the ratio of these two FIR terms gives a number too small to be compatible with simple electron-electron scattering.

Previous low-temperature reflectivity measurements on the HF compounds UBe_{13},[22] $CeCu_6$[23] and UPt_3 (Refs. 24 and 25) reveal anomalous absorptivity in the FIR. Bonn *et al.*,[22] for example, have measured the reflectivity of a polycrystalline UBe_{13} sample over a frequency range extending from 15 to 27 000 cm^{-1} (2 meV to 3.3 eV). Since the dc resistivity is greater than 100 $\mu\Omega$ cm over the whole temperature range studied, the absorptivity is large enough that single-reflection experiments are sufficiently sensitive. In order to perform a Kramers-Kronig analysis to obtain the optical conductivity, the data must extend over all frequency space. At 100 K their low-frequency absorptivity data could be fit with the Hagen-Rubens relation[26] (described in Sec. II) and so extrapolation to zero frequency was possible. At lower temperatures, however, the reflectivity appeared unrelated to the dc resistivity: While the dc resistivity monotonically increased as the temperature decreased from 100 to 2.5 K, the absorptivity displayed a minimum at 50 K below 150 cm^{-1}. Hence various extrapolations were examined, all of which seemed to give stable behavior of the Kramers-Kronig transform above 50 cm^{-1} (6 meV). No explanation was found for the resulting optical conductivity. At 50 K the conductivity below 120 cm^{-1} (15 meV) rises above the dc value, while below this temperature a gaplike structure seems to develop at low frequencies. Since the transformed data only extend to 50 cm^{-1} (6 meV), it is unclear how to interpret these features. From the experiments presented in this paper, it is clear that a knowledge of the conductivity to frequencies below the characteristic energy of the system is essential to an understanding of HF electronic structure.

A measurement of the reflectivity of $CeCu_6$ above 2400 cm^{-1} (300 meV) by Oliver *et al.*[23] is consistent with the findings for UPt_3 presented here. Although dramatic changes in the resistivity and specific heat occur as the HF state develops in going from 12 to 2 K, no change was found in the reflectivity. These measurements provide more evidence that HF behavior must be sought in the low-frequency FIR region.

Marabelli *et al.*[25] recently reported their measurement of the reflectivity of UPt_3 down to 5 K. Using a single reflection off of their sample they obtained the reflectivity from 8 to 4000 cm^{-1} (1 meV to 0.5 eV). By performing a Kramers-Kronig transformation, the complex conductivity is determined from their data. They interpret the resulting low-frequency conductivity as arising from a Drude-like band of free carriers with a band mass of 250 m, containing one electron per formula unit. They fit higher-frequency structure between 30 and 4000 cm^{-1} (4 and 500 meV) with six Lorentz oscillators, attributed to five interband transitions and one optical-phonon mode. The work presented here conflicts at some points with that of Marabelli *et al.* as discussed in Sec. IV.

The experimental techniques and instruments employed to obtain the absorptivity are described in Sec. II, including the development of a highly sensitive FIR coaxial transmission-line technique. Also the relative sensitivity of the various techniques as well as sample preparation are discussed. In Sec. III the absorptivity data for UPt_3 at room temperature and low temperatures are presented along with the results of a complete Kramers-Kronig analysis. In Sec. IV the complex conductivity is analyzed in some detail. A phenomenological model of a frequency-dependent scattering rate is proposed to fit the data in the low-frequency region. A calculation relating the results of this fit to the recent theoretical model for HF systems of Millis and Lee[27] is also presented in this section.

II. EXPERIMENTAL METHODS

Since these measurements span over 4 orders of magnitude in frequency and extend from 1.2 K to room temperature, four instruments are employed to measure the absorptivity. For frequencies above 1000 cm^{-1}, where light intensity is high and good detectors are easy to come by, grating spectrometers are adequate. At room temperature, a Perkin-Elmer grating spectrophotometer is used from 200 to 4000 cm^{-1} with a commercial reflectance attachment. In the range from 3300 to 50 000 cm^{-1} a Cary 17D spectrometer, also with a commercial reflectance accessory, is used.

In the FIR, where intensity is low, the advantages of Fourier-transform spectroscopy are exploited with two step-and-integrate machines. From 50 to 1000 cm^{-1} a Michelson interferometer with a mercury arc provides the FIR radiation and detection is accomplished with a ^{3}He-cooled bolometer. For the lower frequencies, 2–60 cm^{-1}, a lamellar grating interferometer is used in place of the Michelson interferometer.

At room temperature, where the absorptivity is large, the loss from a single reflection at small angle of incidence determined the absorptivity. At low enough frequencies, the absorptivity should be related to the dc resistivity, $\rho_{dc}=\sigma_{dc}^{-1}$, where σ_{dc} is the dc conductivity, by the Hagen-Rubens relation:[26]

$$A=1-R=\left[\frac{2\omega}{\pi\sigma_{dc}}\right]^{1/2} \tag{1a}$$

$$=\left[\frac{2\omega\rho_{dc}}{\pi}\right]^{1/2}. \tag{1b}$$

This equation describes the absorptivity in the classical

skin-effect limit where $\omega\tau \ll 1$ and $l \ll \delta$, with l and δ the electronic mean free path and the classical skin depth, respectively. In words, the electron undergoes many collisions within the skin-depth region and many collisions within each cycle of the driving radiation. For higher frequencies the system passes into the relaxation region where the distance traveled per radian, v_F/ω, of the infrared becomes the important limiting length and the ir field reverses sign before a scattering process occurs ($\omega\tau \gg 1$), giving

$$A = \frac{2}{\omega_p \tau} = \frac{\omega_p}{2\pi\sigma_{\rm dc}} \tag{2a}$$

$$= \frac{\omega_p \rho_{\rm dc}}{2\pi} , \tag{2b}$$

with ω_p the plasma frequency. From Eqs. (1) and (2) it may be seen that, in general, lower resistivity indicates lower absorptivity over the entire frequency range. At still higher frequencies, interband transitions typically dominate the absorptivity.

For the more typical HF systems, such as UBe_{13}, where the resistivity actually increases with decreasing temperature, the absorptivity is large enough that a single-reflection experiment can be made practical. For UPt_3 at 1.2 K, where the resistivity is about 3 $\mu\Omega$ cm, such a measurement is very difficult. Consequently from 10 to 300 cm^{-1} a nonresonant cavity[28] is employed to enhance the effective absorptivity of the sample through multiple bounces. For this experiment the polycrystalline UPt_3 sample forms part of the wall of the nonresonant cavity. At frequencies above 300 cm^{-1} the cavity technique breaks down,[29] indicating a smaller absorptivity than the true value. Thus in the frequency range from 250 to 1000 cm^{-1} the absorptivity is obtained after the incident light makes two reflections from the UPt_3 sample at a 45° angle of incidence.

At the lowest frequencies investigated, from 2 to 30 cm^{-1}, the absorptivity of UPt_3 is so small that even the cavity technique proves inadequate. For this range a transmission-line technique has been developed which achieves an order of magnitude greater sensitivity than the cavity. The concept is based on earlier experimental FIR metal-foil work by Brändli and Sievers.[30] They constructed an array of parallel-plate waveguides with plate separation d much less than the FIR wavelength λ by interleaving metal foil with Teflon or polyethylene spacer material with index of refraction n. By measuring the attenuation through different lengths of the multiwaveguide sample, they extracted the absorptivity of the metal foil. For this geometry, in the limit where $\lambda \ll nd$, ignoring reflections at the ends, the intensity is attenuated by the factor

$$\exp\left[-\left[\alpha(\omega)+\frac{2nr(\omega)}{d}\right]l\right] , \tag{3}$$

where l is the length of the waveguide, α and n are the absorption coefficient and index of refraction of the spacer material, d is the spacing of the plates, and $r(\omega)$ is the ratio of the real part of the surface impedance of the metal foil to the impedance of free space.

Because a foil of UPt_3 cannot be made, a single coaxial waveguide geometry has been chosen. A specially cast 3-mm-diam polycrystalline rod of UPt_3 serves as the center conductor and the outer conductor is machined from oxygen-free high-conductivity (OFHC) copper. A natural weakness of this technique is the enormous loss in throughput, for to ensure the propagation of only the TEM mode the coax must be designed so that the wavelength is much larger than the spacing between the two conductors. With the 1.2-cm-diameter parallel-plate array matched to the same-diameter light pipe, throughput is only reduced by the ratio of the spacer thickness to the sum of the spacer and foil thicknesses. Because the coax geometry corresponds to a single transmission line, expected losses are much greater. With a typical sample diameter of 3 mm and spacing of 0.2 mm, the intensity coming down the $\frac{1}{2}$-in. light pipe is 50 times smaller by geometrical considerations alone. This loss of intensity is mitigated in part by the increased detector sensitivity in low background. By cutting the signal intensity, the sizable background of room-temperature blackbody radiation in the (0–50) cm^{-1} region is also cut and the sensitivity of the ^{3}He-cooled bolometer is raised so that the insertion signal loss is about a factor of 10. This fact, together with the use of carefully constructed input and output coaxial light cones, makes the experiment feasible.

For the coaxial geometry shown in Fig. 1, the intensity of the TEM mode is decreased by the attenuation factor[31]

$$\exp\left[-nr(\omega)\frac{l}{b\ln(a/b)}\right] \tag{4}$$

due to the sample, assuming that the copper absorptivity contribution is negligible at low temperatures. The constants a and b are the radii of the copper outer conductor and the UPt_3 center conductor, respectively. Note that in the limit where the mean radius of curvature, $(a+b)/2$, is much greater than the spacing, $a-b$, Eq. (4) reduces to Eq. (3) (a factor of 2 is absent since, in the case of the coax, the sample only forms one plate).

To demonstrate the improvement over the cavity and single-reflection techniques, consider the error incurred in a measurement of a small absorptivity for an intensity ratio with a 1% error. For the single-reflection $A = 1-R$, a 1% error in R generates an absolute error of ± 0.01 in A. For a cavity,[28] the absorptivity of the sample A_s is calculated from the intensity I_s transmitted through the cavity and the intensity I_r when the samples is replaced with a reference material of known absorptivity A_r by

$$\left[\frac{I_r}{I_s}-1\right] \approx \frac{(A_s - A_r)S_s}{\frac{3}{2}S_h + A_r S_r} . \tag{5}$$

Taking a brass cavity with typical parameter values for the sample area S_s of 1 cm^2, the output coupling hole area S_h of 0.125 cm^2, and cavity surface area S_r of 85 cm^2, an error of ± 0.004 in A is found at 10 cm^{-1}. With the transmission-line technique, using a 25-mm-long sample with a 0.1-mm gap, a 1% error in intensity ratio re-

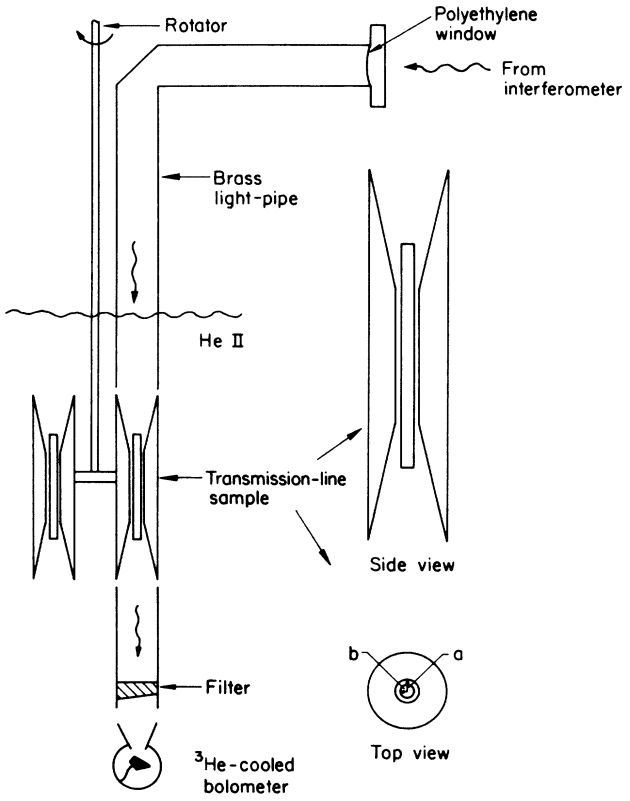

FIG. 1. Schematic diagram of apparatus used in conjunction with the coaxial transmission line. The enlarged views show the transmission line with the UPt_3 center conductor and copper outer conductor. Side view and view down the optical axis. The radius of the inner cylinder is b and the inner diameter of the copper tube is $2a$. The light cones couple the FIR radiation efficiently into the transmission line.

sults in an error of only ± 0.0002 in A.

In practice, as shown in Fig. 1, the transmission of the coaxial UPt_3 sample is referenced to a coaxial copper sample, by rotating the transmission lines into and out of the light pipe. Because of the difficulty in fabricating identical transmission lines, even the ratio of the transmission through two copper coaxial samples can exhibit resonances of $\pm 10\%$. These resonances appear superimposed on the absorptivity of UPt_3 determined at room temperature as well, while the absorptivity determined by a single-reflection technique follows the smooth Drude behavior. Since the structure of these resonances depends on the surface morphology of the samples and the geometry of the transmission line alone, they are temperature independent. Therefore a correction term at 77 K is obtained which is applied to the data at lower temperatures. At 77 K, the absorptivity as determined by the nonresonant cavity technique is large and well described by the Hagen-Rubens relation [Eq. (1)] using the measured dc resistivity. Thus the geometrical resonances in the transmission line can be determined. The measured ratio of the transmission of the coaxial transmission-line sample with the UPt_3 rod compared with that of the Cu rod is composed of a contribution due to the UPt_3 absorptivity and a contribution from the resonances. Subtracting the absorptivity, which is known from the cavity measurement, yields the value of the resonances due to imperfect machining of the transmission lines. Since these corrections are due to effects of the coaxial sample geometry, they are independent of temperature. Hence the effect of the resonances is subtracted out of all of the resulting absorptivity spectra. By referencing the UPt_3 sample transmission to the transmission of a Cu rod sample, any drifts in detector response or changes of detector sensitivity due to coupling of the warm sample to the liquid-helium bath are normalized out.

The polycrystalline UPt_3 rods used in the transmission-line experiments were prepared at the University of California at San Diego (USCD). The original ingot of UPt_3 is prepared by arc-melting the stoichiometric amounts of platinum and depleted uranium, each of 99.9% purity or better, on a water-cooled copper hearth in an atmosphere of high-purity argon. The rods, approximately 40 mm long and 3 mm in diameter, are cast from the ingot in a water-cooled copper split mold. A slight negative pressure is applied to the bottom of the cylinder to draw the molten metal into the mold. After casting, the rods are annealed for 1 week at 800 °C. Measurements on similarly prepared samples show a superconducting transition at a critical temperature of 0.54 K. The measured resistivity value of 3 $\mu\Omega$ cm at 1.2 K for these samples also attests to their quality.

For the higher-frequency experiments (nonresonant cavity and single or double reflections) polycrystalline UPt_3 samples with flat optical surfaces were prepared at Los Alamos National Laboratory. The surfaces were polished to a 0.3-μm diamond grit. Measurements of the ac magnetic susceptibility on samples made from the same batch indicate a superconducting transition. The grain size is typically from 2 to 5 mm for these polycrystalline samples.

While cavities and transmission lines are good for small absorptivities, they have obvious drawbacks, not the least of which are difficulty of operation and the need for specially fabricated samples. In addition, at the present time the transmission lines are limited to frequencies below 30 cm^{-1} by the requirement of $\lambda/2 > d$, where d is the spacing between the inner and outer cylinders of the coaxial transmission line. Cavities begin to saturate at high enough absorptivities, as discussed by Webb.[32] The cavity used by Webb, for example, begins to saturate at an absorptivity of only 2%. Above this point a double-bounce experiment, as described by Webb,[32] may be used.

III. EXPERIMENTAL RESULTS

A. Absorptivity data

The room-temperature absorptivity of UPt_3 over an extended interval is shown in Fig. 2. In the low-frequency regime the data are well fitted with the Hagen-Rubens form [Eq. (1)] as shown by the dashed line. This relation

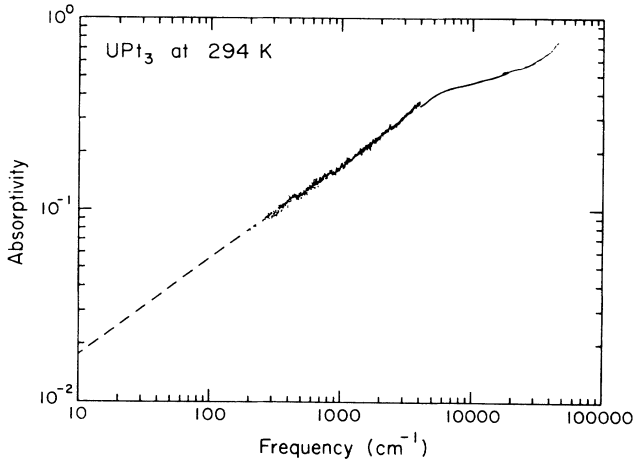

FIG. 2. Normal-incidence absorptivity of UPt_3 as a function of frequency at room temperature. The dashed line is a fit to the Hagen-Rubens form for the low-frequency limit, with a dc resistivity of 255 $\mu\Omega$ cm.

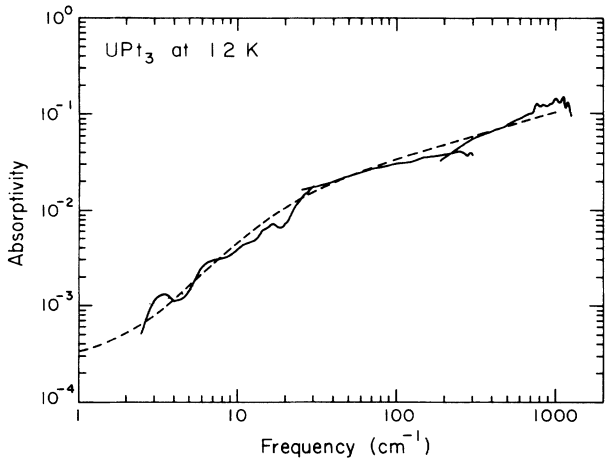

FIG. 3. Absorptivity of UPt_3 at 1.2 K. The resolution is typically 5% of the maximum frequency for each of the three solid curves. The dotted line is the Hagen-Rubens prediction using the measured dc resistivity of 3 $\mu\Omega$ cm. The dashed line results from a fit to a phenomenological model for a frequency-dependent scattering rate, as discussed in the text.

yields a value of 255 $\mu\Omega$ cm for the dc resistivity, in good agreement with published values[33] and measurements of other samples of UPt_3 at Cornell.

Schoenes and Franse[34] have obtained the room-temperature reflectivity of a single crystal of UPt_3 from 240 to 1×10^5 cm^{-1}. Measurements were performed with the electric field vector **E** aligned with either the *a* or *c* axis of the crystal, both of which were contained in the optical surface. For frequencies below 2400 cm^{-1} the reflectivities agreed with the Hagen-Rubens relation using the values of the dc conductivity along the relevant axes. The room-temperature data shown in Fig. 2 are in good agreement with the reflectivity measured with **E** along the *a* axis, for which $\rho_a = 240$ $\mu\Omega$ cm. From a Kramers-Kronig transformations of the data, they give an order-of-magnitude estimate of 1600 cm^{-1} for the width of the Drude free-carrier conductivity and a plasma frequency of 2×10^4 cm^{-1} (2.5 eV) along the *a* axis. They also identify several structures in the conductivity with certain interband transitions in the calculated band structure of Pt by Smith.[35] The room-temperature data of Marabelli *et al.*[25] also agree with those of Schoenes and Franse in the region of overlap (240–4000 cm^{-1}).

Figure 3 shows the measured absorptivity at 1.2 K on a log-log scale from 2 to 1000 cm^{-1}. The three overlapping solid curves were taken with the three techniques previously discussed: coaxial transmission line, nonresonant cavity, and two reflections at 45° angle of incidence. The resolution is approximately 5% of the maximum frequency for each curve. At the lowest frequencies investigated the absorptivity approaches the value predicted by the classical skin effect [Eq. (1)] using the dc resistivity of 3 $\mu\Omega$ cm measured for this sample (the dotted line). At higher frequencies there is a rapid rise to a much larger value of the absorptivity. At frequencies above 20 cm^{-1} the frequency dependence of the absorptivity is the same as that given by the dotted line, but with a larger magnitude. This result indicates that the absorptivity may again be described with Eq. (1), but with a larger effective resistivity.

The FIR absorptivity at two different temperatures is shown in Fig. 4. The comparison demonstrates that above 30 cm^{-1} the absorptivity is relatively temperature independent. The solid curve is the absorptivity at 1.2 K and the dashed curve is taken at 12.5 K. Fewer scans were averaged for the 12.5-K curve causing the degraded

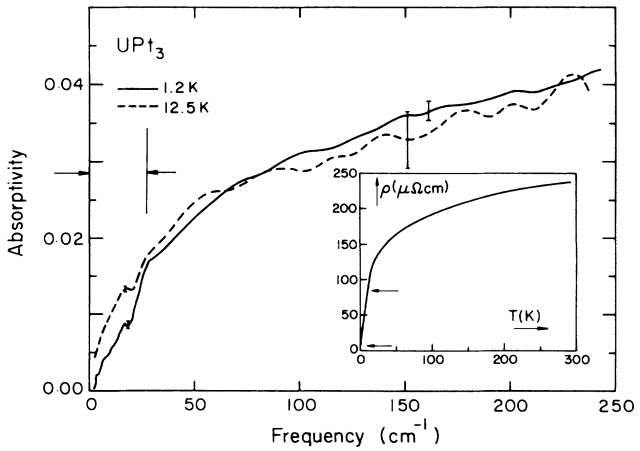

FIG. 4. Absorptivity of UPt_3 at 1.2 K (solid line) and 12.5 K (dashed line) compared. Although by 12.5 K the dc resistivity has risen by more than an order of magnitude over the value at 1.2 K, the absorptivities above 50 cm^{-1} are identical. The vertical bar separates the temperature-dependent region from the temperature-independent region. The inset shows the temperature dependence of the dc resistivity, with arrows indicating the resistivity at 1.2 and 12.5 K.

signal-to-noise ratio for this curve. If one thinks in terms of an effective resistivity as giving rise to the absorptivity above 30 cm^{-1}, this effective resistivity remains constant, independent of the temperature, from 1.2 to 12.5 K. In contrast, the dc resistivity increases by more than an order of magnitude, from 3 to about 80 $\mu\Omega$ cm. The arrows on the inset indicate the two values of the dc resistivity at the two temperatures. The vertical bar on the main figure separates the region of temperature independence on the right from the region of temperature dependence on the left.

A complete temperature-dependent series of the low-frequency absorptivity curves, shown in Fig. 5, demonstrates that below 30 cm^{-1} the absorptivity is very temperature dependent, reflecting the temperature dependence of the dc resistivity. These measurements are made with the coaxial transmission line. In going from 1.2 to 55.6 K, the resistivity climbs from 3 to 170 $\mu\Omega$ cm. Most of the resistivity change is accomplished by 20 K, where the resistivity is 123 $\mu\Omega$ cm. At the lowest two temperatures the absorptivity is compared with the classical skin effect (dashed lines). The measured and calculated curves converge only at the lowest frequencies. As the frequency increases, the absorptivity for the four lowest-temperature curves converges to a single temperature-independent absorptivity, as more clearly shown in Fig. 4. Above 20 K, however, the absorptivity in this frequency region is well described by the classical skin effect [Eq. (1)] using the measured resistivity. The rapid rise of the low-frequency, low-temperature absorptivity to the temperature-independent limit at higher frequencies arises from an increase in the scattering rate as a function of frequency, as will be seen in Sec. IV D. The initial rise is proportional to ω^2, just as the measured dc resistivity for UPt_3 has a term proportional to T^2 at low temperatures.

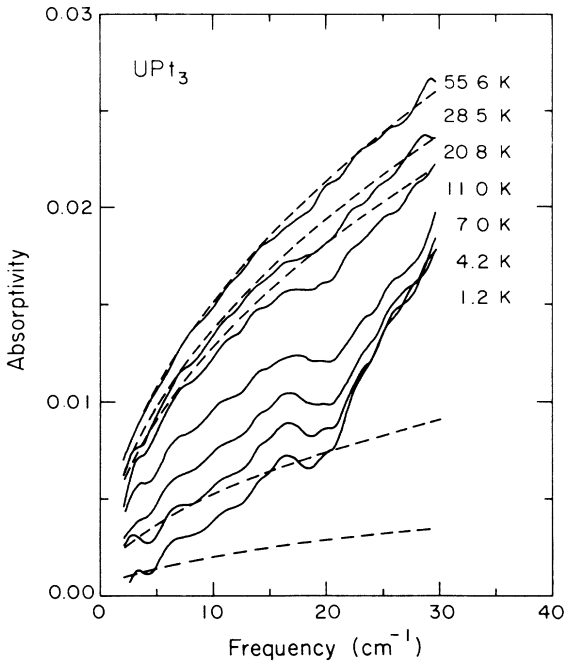

FIG. 5. Absorptivity of UPt_3 vs frequency obtained with coaxial transmission-line technique. Data (solid curves) appear for 1.2 to 55.6 K as labeled. The dashed curves are the Hagen-Rubens prediction using the measured dc resistivity at 1.2, 4.2, 20.8, 28.5, and 55.6 K. The higher-temperature curves follow the dashed curves, while the low-temperature data deviate most strongly at higher frequencies from the dashed curves.

These measurements of the frequency-dependent absorptivity of UPt_3 are in qualitative agreement with those of other researchers on other HF systems:[23,24] Above some frequency of the order of the characteristic energy of the system, the absorptivity is large and not simply related to the dc resistivity. However, these results show that well below this energy scale the absorptivity can be described by the classical skin effect and hence the absorptivity is proportional to the square root of the dc resistivity.

B. Kramers-Kronig analysis

In order to perform a Kramers-Kronig transformation of the data to obtain the complex conductivity, the range of the low-temperature results must be extended beyond 1000 cm^{-1}. Using the recently reported reflectivity data of Marabelli *et al.*[25] for UPt_3 at 5 K, the low-temperature result may be continued to 8000 cm^{-1}. For still larger frequencies, the 300-K data of Schoenes and Franse[34] has been used to reach about 6.4×10^4 (8 eV) and an absorptivity of about 95%. Although the data above 8 eV show that the reflectivity increases again, smoothly extrapolating to 100% absorptivity beyond 8 eV should have little effect in the low-frequency region. This extrapolation is accomplished using an ω^{-4} approximation beyond 8 eV. The low-frequency absorptivity is extrapolated to zero frequency using the Hagen-Rubens relation. The complex conductivity, as obtained by the Kramers-Kronig transform of the composite reflectivity, appears in Fig. 6. The real part of the conductivity is observed to drop rapidly from its zero-frequency value of about 3×10^{16} s^{-1} [33 $(m\Omega\,cm)^{-1}$] to a plateau with a conductivity of 7.2×10^{15} s^{-1} [8 $(m\Omega\,cm)^{-1}$] and then at about 250 cm^{-1} levels off to 2.5×10^{15} s^{-1} [2.8 $(m\Omega\,cm)^{-1}$]. This final plateau value is close to the room-temperature value and the saturation value of the conductivity. As the temperature is raised the low-frequency peak monotonically decreases until the first plateau level is reached and then the conductivity of this plateau decreases to the level of the lowest plateau. The dip in the real part of the conductivity at about 30 cm^{-1} occurs precisely where the transmission-line data and the nonresonant-cavity data overlap, and is probably an artifact of the smooth matching of the two data sets. Above 5000 cm^{-1} the onset of an interband transition occurs. Since the data of Schoenes and Franse have been extrapolated to zero reflectivity above 8 eV to obtain the conductivity in Fig. 6, the magnitude of this interband is much suppressed compared with the interband structures presented by Schoenes and Franse, whose actual data extend to 1×10^5 cm^{-1} (12 eV). Below this interband, however, the conductivity presented here agrees favorably with that of Schoenes and Franse.

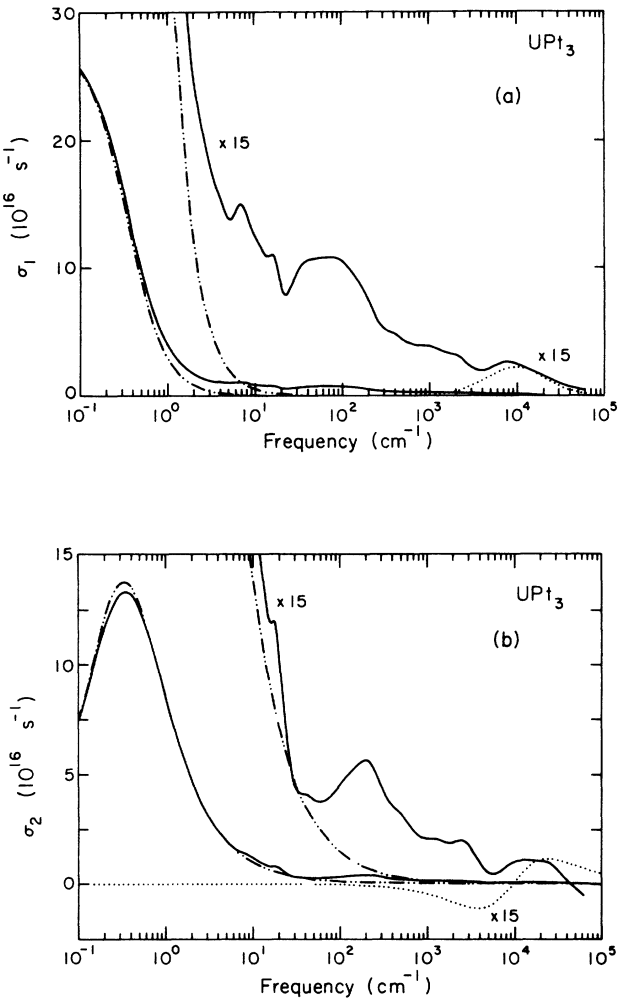

FIG. 6. The complex conductivity of UPt_3 at 1.2 K, as obtained via a Kramers-Kronig transformation of the composite data. The solid lines are the data. The dashed–double-dotted curve is a single Drude-band fit to the low-frequency spike. Also shown is the data multiplied 15×. On this scale, the dotted curve is fitted to a Lorentzian interband. (a) Real part of the conductivity. (b) Imaginary part of the conductivity.

IV. DISCUSSION

In this section the data are first discussed in a general fashion, according to the frequency regime of interest in Secs. IV A and IV B, touching on the high-frequency regime and the FIR regime, respectively. A more detailed analysis of the structure of the conductivity spectrum follows in Secs. IV C and IV D, where two alternative and mutually exclusive means of interpretation are given. Using the general concepts of frequency-dependent scattering developed in Sec. IV D, a simple model fit to the conductivity data is derived in Sec. IV E. Finally in Sec. IV F the current theoretical understanding of heavy-fermion systems is compared with the experimental data.

A. High-frequency region

With the complex conductivity determined, the identification of the free carriers and bound carriers can proceed. In Fig. 6 the feature in σ_1 centered at about 1×10^4 cm^{-1} is assigned to an interband transition. A Lorentzian centered at 9500 cm^{-1} with a width of 20 000 cm^{-1} fits quite well, as shown by the dotted line in Fig. 6. As mentioned above, including the actual reflectivity beyond 6.4×10^4 cm^{-1} (8 eV), which rises from its minimum value of about 5%, leads to a much larger and broader interband in the conductivity of Schoenes and Franse.[34] They identify several closely spaced interband transitions within this feature. Since the purpose here is merely to obtain an estimate of the plasma frequency, a single Lorentzian is sufficient. Subtracting off this single Lorentzian allows an estimate of the plasma frequency associated with the remaining carriers. Integrating the area under the conductivity without the interband and using the sum rule[26]

$$\int_0^\infty \sigma_1(\omega)d\omega=\omega_p^2/8 \tag{6}$$

gives a plasma frequency of 2.1×10^4 cm^{-1} or 2.6 eV. Schoenes and Franse quote 2.5 eV as their estimate of the plasma frequency. At 1.2 K, what remains in the conductivity after the interband is removed is not a simple Drude free-carrier peak, although at room temperature the remainder is approximately Drude. Rather, there is a great deal of structure, as has been mentioned in the preceding section. The remainder of this Discussion section focuses on the proper interpretation of this structure.

Webb, Sievers, and Mihalisin[18] found a qualitatively similar behavior in the low-temperature conductivity of the VF compound $CePd_3$. They observed a narrow (1 cm^{-1} wide) peak with high conductivity which gave way to a plateau of much lower conductivity at higher frequencies. Although the structure observed for UPt_3 appears somewhat more complicated, the behaviors of the two systems no doubt arise from the same physical interactions.

B. FIR Region

The reflectivity results of Marabelli *et al.*[25] in the FIR region are in good agreement with the findings presented in this paper for frequencies above 50 cm^{-1}. This allows for a smooth match of the high-frequency data shown in Fig. 3 onto theirs as discussed in Sec. III. However, below this frequency they observe a large maximum in the absorptivity at about 20 cm^{-1}. Upon obtaining the complex conductivity via a Kramers-Kronig transformation of their data, they find a maximum in the real part of the conductivity at 32 cm^{-1}, resulting from the maximum in absorptivity. From this complex conductivity they conclude that in UPt_3 there is a Drude-like band of carriers with a band mass of about 250 m and an interband transition with a maximum at 32 cm^{-1}. This interpretation of the electronic structure of UPt_3 results from the maximum they observe in the absorptivity at about 20 cm^{-1}. The region in which the two experimental results differ is exactly that range which is most difficult for

a single-reflection experiment, the technique used by Marabelli *et al.*, as the reflectivity is high and the blackbody source is at its weakest. The measurement presented here, which uses the more sensitive transmission-line technique, shows no such maximum, only a monotonic decrease to zero absorptivity at zero frequency.

Marabelli *et al.* interpret a minimum in their conductivity at 14 cm^{-1} as arising from the fortuitous overlap of the Drude free-carrier tail with an interband transition having its maximum at 32 cm^{-1}. Since the data discussed in this paper go to 1.2 K, where the dc conductivity is an order of magnitude greater than at 5 K, the Drude tail of the free carriers should be reduced by an order of magnitude where the free-carrier band overlaps the interband, enabling such a structure to be resolved. No structure is seen hence the data do not support the interpretation of Marabelli *et al.*

Two basic schemes of interpretation of the data in Fig. 6 are possible. First the conductivity may be parametrized with a set of different free or bound carriers—a multiband model (for an extreme example, see Marabelli *et al.*). Alternatively, the Drude model can be generalized and the behavior ascribed to a single set of free carriers with a frequency-dependent scattering rate defined by $\Gamma(\omega)=\Gamma_1(\omega)+i\Gamma_2(\omega)$.

C. Multiband model

In the multiband scheme, the general features of the conductivity can be reproduced by the sum of three Drude bands, each with conductivity

$$\sigma(\omega)=\frac{ne^2\tau}{m_b}\frac{1}{1-i\omega\tau}=\frac{\sigma_0}{1-i\omega\tau}\ , \tag{7}$$

with the parameters σ_0 and τ given in Table I. The charge carriers in each band are described by a number density n, a band mass m_b, and a scattering rate $1/\tau$. From such a Drude band fit only the ratio of n to m_b is obtained. By using the low-temperature specific-heat data as an additional piece of information, however, the values of n and m_b within the free-electron model may be determined. Fitting the specific heat to the free-electron form,

$$C(T)=\gamma T+\beta T^3\ , \tag{8}$$

the experimentally measured specific heat[36] gives a γ value for UPt_3 of 422 mJ/mol K^2. According to the free-electron model, γ is related to the effective mass and the Fermi wave vector by[37]

$$\gamma=\frac{1}{3}\left[\frac{k_B}{\hbar}\right]^2 m^* k_F V\ , \tag{9}$$

where V is the molar volume[38] of 42.4 cm^3 for UPt_3. Since there are no mass-enhancement mechanisms in the multiband model, the effective mass m^* and the band mass m_b are identical. If it is assumed that the first band gives rise to the large value of γ, the band mass and the carrier density can be calculated from Eqs. (7) and (9). These relations yield 1.25 electrons per formula unit and an m_b/m of 240. Alternatively, the first band could be ignored and the second or third band assumed to dominate the specific heat. This case gives seven electrons per formula unit with an m_b/m of 135 for the second band or 27 electrons per formula unit and an m_b/m of 85 for the third band. Clearly the specific heat must be ascribed to the first band.

Since only the plasma frequency for the second and third Drude bands is known, only $(m_b/m)/z$ can be calculated, where z is the number of electrons per formula unit in each band. Thus in attempting to calculate the mean free path $l=v_F\tau$, a value for z (or equivalently m_b/m) must be assumed for the second and third bands. Assuming one electron per band ($z=1$) gives mean free paths of 580, 12, and 6.1 Å for the three bands. In Table I, a range of l is indicated. The lower values for the mean free path are calculated assuming $z=2$, a reasonable upper limit on the number of electrons. The higher values for the mean free path are calculated assuming $m_b/m=1$.

The major shortcoming of this model is that there is no predicted temperature dependence, while the strength of the frequency-dependent scattering model, as shown below, lies in the correlation of frequency- and temperature-dependent behavior. The appearance of such disparate mean free paths also weakens the case for this three-band model.

D. Frequency-dependent scattering

Consider now the case of a single band in which the free carriers are scattered at a frequency-dependent scattering rate, so that the complex conductivity may be written

$$\sigma(\omega)=\frac{\omega_p^2/4\pi}{\Gamma(\omega)-i\omega}\ . \tag{10}$$

TABLE I. Parameters for a three-band model that gives the general features of the conductivity. The plasma frequency ω_p may be calculated from the dc conductivity σ_0 and the scattering time τ within the Drude model. From ω_p only the ratio of the band mass, m_b, to the number of electrons per formula unit, z may be determined. Note especially the wide variation in the mean free paths l between the three bands.

Band	σ_0 (s^{-1})	τ (s)	ω_p (s^{-1})	$(m_b/m)/z$	l (Å)
1	2.76×10^{17}	1.5×10^{-11}	4.8×10^{14}	200	580
2	4.65×10^{15}	2.7×10^{-14}	1.5×10^{15}	20	7.6–88
3	2.5×10^{15}	2.2×10^{-15}	3.8×10^{15}	3.1	3.8–13

Let Γ_2 be identified with a self-energy correction to the quasiparticle effective mass and define

$$\omega\lambda(\omega)=-\Gamma_2(\omega)\ , \tag{11}$$

where $1+\lambda$ is the frequency-dependent mass-enhancement factor; hence,

$$m^*(\omega)=m_b[1+\lambda(\omega)]\ , \tag{12}$$

where m_b is the band mass. This identification arises from rewriting Eq. (10) in the Drude form with a new renormalized frequency-dependent (real) scattering rate and plasma frequency:

$$\sigma(\omega)=\frac{\omega_p^{*2}/4\pi}{1/\tau^*(\omega)-i\omega} \tag{13}$$

with

$$\frac{1}{\tau^*}=\frac{\Gamma_1}{1+\lambda} \quad \text{and} \quad \omega_p^{*2}=\frac{\omega_p^2}{1+\lambda}\ .$$

Then, from the measured conductivity the two frequency-dependent quantities may be extracted as follows:

$$\Gamma_1(\omega)=\frac{\omega_p^2\sigma_1}{4\pi\,|\,\sigma\,|^2} \tag{14}$$

and

$$1+\lambda(\omega)=\frac{\omega_p^2\sigma_2/\omega}{4\pi\,|\,\sigma\,|^2}\ . \tag{15}$$

From the complete measured complex conductivity, $\Gamma_1(\omega)$ and $1+\lambda(\omega)$ are calculated and plotted in Figs. 7 and 8. Since the sum-rule approach described in Sec. IV A only gives an estimate of the plasma frequency, the plots are left with the ordinate scale in terms of $4\pi/\omega_p^2$. In Fig. 7(a) the real part of the scattering rate as a function of frequency is plotted on a log-log scale to give the overall picture. There are three plateau regions, just as in the real part of the conductivity. The highest plateau is somewhat distorted due to the presence of the interband. Since the low-frequency region exhibits most dramatic variation of the scattering rate, the same curve is plotted over a restricted frequency range with a linear scale in Fig. 7(b). The scattering rate begins at the small dc value then rises rapidly to a remarkably flat plateau above 30 cm^{-1}. Webb, Sievers, and Mihalisin[18] observed qualitatively similar behavior for the scattering rate of $CePd_3$. The characteristic energy scale is an order of magnitude greater for $CePd_3$, however, with the scattering rate reaching half of its maximum value at about 140 cm^{-1} instead of 14 cm^{-1} for UPt_3 as shown in Fig. 7(b).

The mass enhancement $1+\lambda$ on a log-log scale is given in Fig. 8(a). This parameter drops dramatically as the frequency is increased. At higher frequencies the enhancement is driven negative by the interband. In Fig. 8(b) the enhancement is shown on a linear scale with the same frequency axis as in Fig. 7(b) for comparison. The enhancement drops off at a characteristic frequency of about 12 cm^{-1}, and then remains flat.

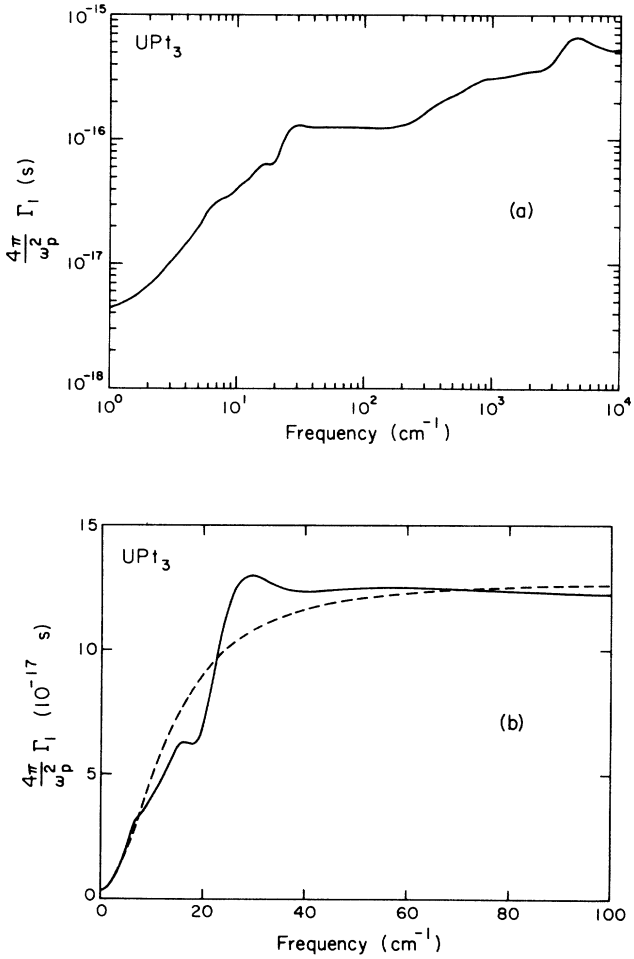

FIG. 7. The frequency-dependent scattering rate at 1.2 K as derived from the complex conductivity as discussed in the text. (a) shows the scattering rate over the whole frequency region. (b) shows the scattering rate from 0 to 100 cm^{-1}. The dashed line is the phenomenological model of a frequency-dependent scattering rate as obtained from a fit to the absorptivity in Fig. 3.

Within this framework of frequency-dependent scattering, the data may be used to obtain the relevant free-electron parameters, namely the number density n, the bare optical band mass m_b, and the mass-enhancement factor $\lambda(0)$, which arises from interactions which dress the bare electron mass. The first step in the analysis is to estimate the bare plasma frequency. This estimate is obtained in Sec. IV A using the sum rule given in Eq. (6). This bare plasma frequency depends only on the ratio of the number density n to the bare optical band mass m_b since

$$\omega_p^2=\frac{4\pi ne^2}{m_b}\ . \tag{16}$$

With this plasma frequency, the intercept in Fig. 8 may be used to find a value for the zero-frequency mass-enhancement factor $\lambda(0)=65$. This is a measure of the

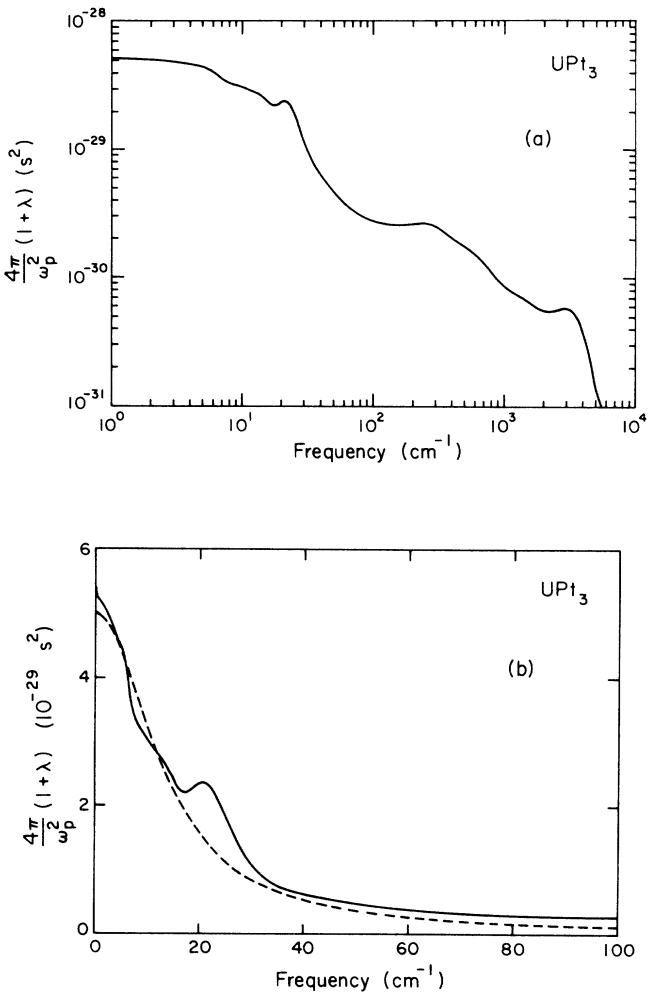

FIG. 8. The frequency-dependent mass enhancement at 1.2 K as derived from the complex conductivity as discussed in the text. (a) shows the mass enhancement over the whole frequency region. (b) shows the mass enhancement from 0 to 100 cm^{-1}. The dashed line is the phenomenological model of a frequency-dependent scattering rate as obtained from a fit to the absorptivity in Fig. 3.

strength of the interactions which dress the bare optical mass, resulting in an enhanced low-frequency mass. Thus the effective low-frequency mass may be written as the product of the bare optical band mass and the enhancement factor, so that

$$m_0^* = [1+\lambda(0)]m_b \ . \tag{17}$$

In order to obtain the free-electron model parameters n and m_b another piece of data is required, since only the ratio of these parameters is known from the bare plasma frequency. For this step of the analysis, the γ value from the specific heat provides the necessary additional information, since within the free-electron model [Eq. (9)] γ has a different functional dependence on n and m_b than the bare plasma frequency. If it is assumed that the low-frequency FIR mass is equal to the specific-heat thermal mass, i.e., $m_0^* \approx m^*$ (see Webb, Sievers, and Mihalisin[18]), then from Eqs. (9), (16), and (17) and the specific-heat γ value[36] of 422 mJ/mol K^2, the band mass and the Fermi wave vector may be evaluated within the isotropic quasiparticle approximation. The results are that $m^* = 237$ m, $m_b = 3.7$ m, and $k_F = 8.1 \times 10^7$ cm^{-1}. This value for k_F yields a free-carrier density of $n = 1.8 \times 10^{22}$ cm^{-3} which corresponds to 1.25 electrons per formula unit, in agreement with the value of one conduction electron per formula unit inferred from the Hall measurement for UPt_3 recently reported by Schoenes and Franse.[39]

E. Phenomenological model

In order to obtain quantitative values of parameters which may be compared with theory, the absorptivity is fit with a simple model for the frequency-dependent scattering rate motivated by the results shown in Figs. 7 and 8. As the frequency approaches zero, the scattering rate must approach the value given by the dc resistivity, as is borne out by the data. At higher frequencies, the absorptivity is again proportional to the square root of the frequency, indicating that the scattering rate saturates. Of course, from general considerations of unitarity the scattering rate must eventually saturate.[40] At the lowest temperatures, the resistivity has a T^2 term, possibly arising from electron-electron or electron–spin-fluctuation interactions. This rise with T^2 in the scattering rate implies a similar rise with the square of frequency at the lowest frequencies. The simplest frequency-dependent scattering rate which has the correct limiting forms is

$$\Gamma(\omega) = \Gamma_d + \frac{\lambda_0 \omega^2 \alpha}{1+\omega^2\alpha^2} \ , \tag{18}$$

where Γ_d is the dc scattering rate, $1+\lambda_0$ is the low-frequency mass enhancement, and $1/\alpha$ is a characteristic frequency of the process. Via Kramers-Kronig considerations, this frequency-dependent scattering gives rise to a concomitant renormalization of the mass given by

$$\lambda(\omega) = \frac{\lambda_0}{1+\omega^2\alpha^2} \ . \tag{19}$$

Fitting the UPt_3 absorptivity data at 1.2 K to this form of the scattering rate produces good agreement over almost 3 orders of magnitude in frequency (see dashed line in Fig. 3). In Fig. 3 the dashed line (the phenomenological model) falls below the dotted line (the Hagen-Rubens prediction) because, just before the scattering rate "turns on," the relaxation regime is entered ($\omega\tau > 1$), reducing the absorptivity below the classical skin-effect value. At lower frequencies the dashed line converges to the classical skin-effect prediction. Since the fit to the data is over a restricted frequency interval, a unique value for ω_p cannot be obtained and, hence, Table II gives the fitting parameters for three different values of ω_p, in order to demonstrate the dependences of the parameters on the choice of plasma frequency. Because the plasma frequency of the first fit recorded in Table II is close to that estimated in Sec. IV A from the sum rule, these parameters

TABLE II. Four parameters of a simple model of a frequency-dependent scattering rate that is fitted to the absorptivity in Fig. 3. Because of the restricted frequency interval of the fit, a unique value for ω_p cannot be obtained, hence the fitting parameters for three different values of ω_p are shown. However, the value of $1/\alpha$ remains relatively constant independent of ω_p, as does the ratio of $\omega_p^2/(1+\lambda_0)$. The Γ_d value is calculated using ω_p and the dc resistivity.

ω_p (cm^{-1})	λ_0	$1/\alpha$ (cm^{-1})	Γ_d (cm^{-1})
2.11×10^4	65±8	15±1	24
3.39×10^4	162±20	13.3±1	60
6.18×10^4	510±40	12±1	200

are used to obtain the dashed curve in Fig. 3, and are used in the discussion. The values for Γ_d in the table are derived from the particular plasma frequency and the measured dc resistivity. Since each set of parameters gives an equally good fit to the data, a unique value cannot be obtained for the mass enhancement at zero frequency from such a fit. However, if the estimate of the plasma frequency is increased (column 1), the value of the mass enhancement also increases (column 2), roughly as the square of ω_p. Thus, as long as $\omega_p^2/(1+\lambda_0)=7.2\times10^6$ cm^{-2}, a good fit is obtained. From Fig. 7, obtained from the Kramers-Kronig analysis, a zero-frequency value of 6.7×10^6 cm^{-2} for $\omega_p^2/(1+\lambda_0)$ is found, which is close to the value obtained from the fit of the model to the absorptivity. The values are not identical since the value obtained from the phenomenological fit results from fitting a simplified form to the data over a wide frequency range, while the zero-frequency value obtained from Fig. 7 reflects the actual behavior only at low frequencies. Inspection of Table II also shows that $1/\alpha$ is fairly independent of the plasma frequency, with $12 < 1/\alpha < 15$ cm^{-1}. The fit of the model using the first set of parameters from Table II is shown as the dashed curves in Figs. 7(b) and 8(b).

This frequency-dependent scattering rate is interpreted as arising from the coupling of the itinerant electrons to the spin-fluctuation spectrum, which dresses the electrons giving them a large effective mass at low frequencies. At energies higher than $1/\alpha$ the electrons are unscreened, revealing the bare optical band mass, and so scatter off of the spin fluctuations. In comparison to $CePd_3$, the more complicated structure of the conductivity seen in Fig. 6, resulting from the rise of the scattering rate to a second plateau above 1000 cm^{-1} as shown in Fig. 7(a), may arise from the highly anisotropic Fermi surface predicted by some band-structure calculations.[2]

The observation of a large increase in the scattering rate at an energy $1/\alpha$ of order 10 cm^{-1} is in agreement with the observation of structure in numerous properties of UPt_3 at this same energy scale. For example, at about 7 K there is a maximum in the slope of the dc resistivity[19] and a maximum in the thermopower.[33] At 11 K there is a maximum in the thermal-expansion coefficient[41] and at 10 K a maximum in the slope of the magnetic susceptibility.[42] The Hall coefficient begins to drop linearly to near zero beginning around 20 K.[43] Fitting the specific heat to the spin-fluctuation model with a $T^3\ln(T)$ term gives a T_{SF} of about 26 K.[44] Recently, a peak has been observed in the longitudinal-acoustic attenuation at 12 K for UPt_3.[45] These observations are summarized in Table III. Clearly something important is occurring in the HF state on this energy scale.

F. Comparison with theory

It has been shown here that the FIR absorptivity may be explained by a frequency-dependent scattering rate with an initial ω^2 frequency dependence. In addition, several dc measurements[19–21] have demonstrated a T^2 temperature dependence in the resistivity at low temperatures. If these two effects have their source in the same scattering process, then their relative magnitudes should be related in a very general way. Several scattering processes which give rise to T^2 and ω^2 scattering rates have been proposed as the relevant mechanism for HF systems. Phase-space arguments[46] within the Fermi-liquid framework constrain the ratio of the T^2 and ω^2 terms, so that all of the theories mentioned have the same relative size of these terms in the scattering rate. The observed relative size of the ω^2 term is much larger than the theoretical value, as will be seen. Preliminary attempts at using a quasiclassical Boltzman approximation[47] indicate that corrections to this ratio act to increase the relative size of the ω^2 term.

Electron-electron scattering is considered first. The imaginary part of the self-energy of the electron due to the electron-electron interaction and the correctly renormalized phonon-mediated electron-electron interaction in the low-frequency and low-temperature limit has the form[48]

$$\mathrm{Im}\Sigma(\omega,T)\propto\omega^2+(\pi T)^2 . \tag{20}$$

This self-energy term is related to the single-particle scattering rate $1/\tau(E)$ by

$$\frac{1}{\tau(E)}=-2\,\mathrm{Im}\Sigma(E) , \tag{21}$$

where E is the energy of the electron relative to the Fermi energy. The scattering rate used to determine the

TABLE III. Summary of some experiments that have identified characteristic temperatures for UPt_3, as discussed in the text.

Property	Behavior	T (K)	Ref.
Resistivity	Max. in slope	7	19
Thermopower	Max.	7	33
Thermal-expansion coefficient	Max.	11	41
Magnetic susceptibility	Max. in slope	10	42
Hall coefficient	Changes behavior	20	43
Specific heat	T_{SF} from fit	26	44
Longitudinal-acoustic attenuation	Max	12	45

complex conductivity follows from a proper averaging of this single-particle scattering rate. Murata[49] derived a formula for the optical conductivity for s-wave scattering which performs the proper average:

$$\sigma(\omega)=\frac{ne^2}{m}\int\frac{[f(E-\omega)-f(E)]/\omega}{i\Sigma(E)-i\Sigma^*(E-\omega)-i\omega}dE\ , \tag{22}$$

where $f(E)$ is the Fermi function $(e^{\beta E}+1)^{-1}$. This relation takes into account that a photon of energy ω excites an electron out of the Fermi sea to an energy E, creating a hole of energy $E-\omega$. The single-particle scattering rate for this electron, $1/\tau(E)$, then depends on the final energy E of the electron. At $t=0$ the photon may excite electrons which are within $\hbar\omega$ of the Fermi surface; thus the integral reflects an averaging of single-particle scattering rates from $1/\tau(0)$ to $1/\tau(\omega)$. For temperatures greater than zero, electrons exist above the Fermi surface and the average extends over all frequencies with a proper weighting by the Fermi functions. Allen[50] proposed a similar form for the conductivity for the electron-phonon interaction. If the single-particle scattering rate is a constant τ_0, then the Murata formula reduces to the Drude model:

$$\sigma(\omega)=\frac{ne^2}{m}\frac{1}{1/\tau_0-i\omega}\ . \tag{23}$$

Gurzhi[51] has calculated the electron-electron scattering rate to be

$$\Gamma(\omega,T)\propto\omega^2+(2\pi T)^2\ . \tag{24}$$

From this relationship [Eq. (24)] and the frequency dependence of the absorptivity in the FIR [Eq. (18)] a value of about 15 $\mu\Omega\,\mathrm{cm/K^2}$ is calculated for the coefficient of the T^2 term in the resistivity. Experimental values are much smaller ranging from 1.6 to 3 $\mu\Omega\,\mathrm{cm/K^2}$.[19–21] Alternatively, an experimental scattering rate may be written:

$$\Gamma_{\mathrm{expt}}(\omega,T)\propto\omega^2+(p\pi T)^2\ . \tag{25}$$

From the data an upper limit of $p=1$ may be determined.

Riseborough[52] has calculated the frequency-dependent scattering due to spin fluctuations and has found a T^2 contribution to the resistivity. His form of the scattering rate also reduces in the low-frequency and low-temperature limit to Eq. (24).

Millis and Lee[27] have recently developed a formalism to study the low-temperature properties of the lattice Anderson Hamiltonian. This Hamiltonian is believed to contain all of the essential physics of HF and VF systems. Millis and Lee find a nonmagnetic ground state that behaves as a Fermi liquid with a large effective mass. Their evaluation of the complex conductivity and the imaginary part of the quasiparticle self-energy is particularly relevant to the work presented in this paper. In the $U=\infty$ limit, where U is the Coulomb repulsion between f electrons on the same site, the Hamiltonian may be written:

$$H_A=\sum_{k,\sigma}\varepsilon_{k\sigma}c^\dagger_{k\sigma}c_{k\sigma}+\sum_{i,m}E_{0m}f^\dagger_{im}f_{im}+\sum_{k,i,m,\sigma}(Ve^{ikR_i}c^\dagger_{k\sigma}f_{im}+\mathrm{H.c.})\ . \tag{26}$$

This Hamiltonian describes a band of conduction electrons with operator $c_{k\sigma}$ and energy $\varepsilon_{k\sigma}$ which hybridizes with a set of localized f electrons with operator f_{im} and energy E_{0m} via an interaction V, taken to be a constant for simplicity. The solution is subject to the constraint that each site may be occupied by at most one f electron (the $U=\infty$ limit):

$$\left\langle\sum_m f^\dagger_{im}f_{im}\right\rangle\equiv\langle n^i_f\rangle\le 1\ . \tag{27}$$

Since the constraint does not commute with H_A, and hence cannot be maintained in time, a slave-boson field $b^\dagger_i$ is introduced which creates a hole on the site i whenever an f electron is removed from the site. This results in a new hybridization term in H_A and a new constraint equation which does commute with H_A:

$$\sum_{k,i,m,\sigma}(Ve^{ikR_i}c^\dagger_{k\sigma}f_{im}b^\dagger_i+\mathrm{H.c.}) \tag{28}$$

and

$$\langle Q_i\rangle\equiv\langle n^i_f\rangle+\langle b^\dagger_i b_i\rangle=1\ . \tag{29}$$

This Hamiltonian is then analyzed using conventional quantum-field-theoretical techniques including a $1/N$ expansion, where N is the orbital degeneracy of the f state. The $1/N$ expansion leads to the identification of an energy parameter ε_f which is analogous to the Debye frequency in the electron-phonon–interaction problem, in that it sets the scale for the energy of the boson propagator. However, unlike the electron-phonon problem, ε_f is also the Fermi energy of the final ground-state. Assuming a mean-field solution leads to a Kondo-like relation for ε_f:

$$\varepsilon_f=W\exp\left[\frac{E_0}{\rho_0V^2}\right]\ , \tag{30}$$

where W is the conduction-electron bandwidth and ρ_0 is the conduction-electron density of states per spin (of order $1/W$). This solution gives very flat bands at the Fermi surface, resulting in the large effective mass:

$$\frac{m^*}{m}=\frac{1}{N\varepsilon_f\rho_0}\approx\frac{W}{N\varepsilon_f}\ . \tag{31}$$

Evaluating the conduction-electron Green function for low frequencies, $\omega\ll\varepsilon_f$, results in the form

$$G_c(k,\omega)=\frac{Z}{\omega-v^*_F|k-k_F|}\ , \tag{32}$$

where

$$Z=(1+m^*/m)^{-1}\ . \tag{33}$$

At much higher frequencies the conduction-electron Green function is that of the unhybridized conduction electron. Calculating the first $1/N$ correction term to the

Green function, Millis and Lee find the imaginary part of the self-energy Σ_c at low frequencies (using the relation $G_{c,\text{full}}{}^{-1}=G_c^{-1}-\Sigma_c$,

$$\text{Im}\Sigma_c(\Omega,T)=\frac{n_f}{N}\frac{m^*}{m}\frac{\Omega^2+\pi^2T^2}{\varepsilon_f} . \tag{34}$$

This form for the self-energy results in the same ratio of the frequency- and temperature-dependent contributions to the scattering rate as calculated by Gurzhi [Eq. (24)], which is not in quantitative agreement with the experiment as previously discussed. Including impurity scattering, they find that at very low frequencies and temperatures, where the electron-boson scattering expressed by Eq. (34) is negligible, the real part of the conductivity is given by

$$\sigma_{1i}(\omega)=\frac{ne^2\tau_i}{m[1+(m^*/m)^2\omega\tau_i^2]}$$
$$=\frac{ne^2\tau_i^*}{m^*(1+\omega^2\tau_i^2)}, \quad \omega<\varepsilon_f \tag{35}$$

with

$$\tau_i^*=\frac{m^*}{m}\tau_i . \tag{36}$$

Millis and Lee conclude that at $T=0$ the dc resistivity of HF compounds should be similar to that of a conventional metal with similar purity. The frequency dependence predicted by their model, however, is dramatically different. For HF compounds the predicted conductivity can roll off at a fraction of a wave number, while for normal metals of similar resistivity the roll off is at several hundred wave numbers.

At higher frequencies the model conductivity saturates at

$$\sigma_1(\omega)=\frac{ne^2}{mN\varepsilon_f(m^*/m)}\approx\frac{ne^2}{m}\frac{1}{W} . \tag{37}$$

Excellent qualitative agreement is found between the experimental results for UPt_3 and the theory of Millis and Lee. If $N\varepsilon_f$ is identified with the parameter $1/\alpha$, m^*/m with $1+\lambda_0$ and $1/\tau_i$ with Γ_d, then the empirical fit for the conductivity [Eqs. (18) and (19) in Eqs. (10) and (11)] reduces to the forms given by Millis and Lee in Eqs. (32) and (34). Using the values of $1/\alpha$, ω_p, and λ_0 from Table II in Eq. (37) an estimate of 110 $\mu\Omega$ cm is found for the high-frequency saturation resistivity, while the actual value is 360 $\mu\Omega$ cm. This estimate seems reasonable, considering the simplicity of the model, especially in the light of the complicated Fermi surface predicted from band-structure calculations.[2] From Eq. (31), the conduction-electron bandwidth is estimated to be 0.1 eV, or, equivalently, a density of states (DOS) per spin of 136 states/Ry. Assuming two spin states, the total DOS is 272 states/Ry, while Oguchi and Freeman calculate[2] a value of 114 states/Ry. These results are summarized in Table IV. The success of the model of Millis and Lee in qualitatively describing the frequency dependence of the conductivity and in relating the relevant energy scale $N\varepsilon_f$ and mass m^*, to the saturation resistivity, bandwidth, and temperature dependence of the resistivity supports the essential correctness of their theory.

While a two-band model can mimic the behavior of the simple frequency-dependent scattering rate chosen here, there are some important differences. Chief among them is that the two-band model gives no *a priori* relation between the temperature and frequency dependence of the scattering rate. That the experimental results agree with the theoretical predictions of Millis and Lee lends much support to the choice of a frequency-dependent scattering rate over other interpretations. Of course, the lack of exact quantitative agreement demonstrates the need for further development of the theory to include a more realistic initial band structure. Also, a more detailed calculation of the scattering rate should improve the agreement between the experimental and theoretical values of the scattering rate.

A final point of interest concerns the saturation value of the scattering length at high frequencies. For UPt_3 a value of roughly 5 Å is calculated, which is close the U-U separation.[1] For the valence fluctuator $CePd_3$ similar experiments yield a saturation scattering length closer to the Ce-Ce distance.[18] Thus in both cases the scattering saturates when the scattering length is equal to the separation of the f-electron sites.

V. CONCLUSIONS

In some respects the valence fluctuator $CePd_3$ and the heavy-fermion UPt_3 differ only in the energy scale, set by $N\varepsilon_f$. Table IV presents a comparison of the two systems. The value of about 140 cm^{-1} for $N\varepsilon_f$ and λ_0 of 40 in $CePd_3$ lead to a DOS of 39 states/Ry, which is smaller than that of UPt_3. Both systems exhibit a T^2 term in the resistivity with the theory of Millis and Lee[27] predicting 1.1 $\mu\Omega\,\text{cm/K}^2$, a fair estimate for HF theories to the published[53] value of 0.085 $\mu\Omega\,\text{cm/K}^2$. However, differences do exist between UPt_3 and $CePd_3$. While the saturation

TABLE IV. Comparison of the theory of Mills and Lee with experiment for the high-frequency saturation value of the resistivity, ρ_{sat}, the T^2 coefficient of the resistivity, A, and a band-structure calculation of the total density of states (DOS) at the Fermi surface. The data for $CePd_3$ of Webb, Sievers, and Mihalisin (Ref. 18) is presented for comparison with UPt_3.

	ω_p (s^{-1})	$N\varepsilon_f=1/\alpha$ (cm^{-1})	$\lambda_0=m^*/m$	ρ_{sat} ($\mu\Omega$ cm) Theor.	Expt.	A ($\mu\Omega\,\text{cm/K}^2$) FIR Expt.	dc Expt.	DOS (states/Ry) Theor.	Calc.
UPt_3	3.9×10^{15}	13	65	110	360	15	1.6–3	272	114
$CePd_3$	3.34×10^{15}	140	40	1000	1100	1.1	0.085	39	

value of the resistivity for high frequencies is the same as the high-temperature saturation value of the resistivity for UPt_3, this is not the case for $CePd_3$. Instead, $CePd_3$ has a maximum resistivity of about 180 $\mu\Omega$ cm in temperature, but the high-frequency saturation value for the resistivity at 4.2 K is about 1000 $\mu\Omega$ cm. In some sense the behavior of the resistivity of $CePd_3$ with temperature, with its maximum at about 130 K, is more reminiscent of UBe_{13} and other more typical HF systems than of UPt_3, with its simple monotonic behavior. Nonetheless, the comparison presented in Table IV is compelling evidence in favor of the theory of Millis and Lee.

With the insight into the relationships among the various properties of the HF state provided by Millis and Lee, the important energy scale for other HF compounds now can be estimated. The coefficient of the T^2 term in the resistivity, A, varies as

$$A \propto \frac{4\pi}{\omega_p^2}\lambda_0\alpha \tag{38}$$

and the saturation value of the resistivity for high frequency is given by

$$\rho_{\rm sat}=\frac{4\pi\lambda_0}{\omega_p^2\alpha} . \tag{39}$$

Combining these two properties gives

$$\frac{\rho_{\rm sat}}{A} \propto \left[\frac{1}{\alpha}\right]^2 . \tag{40}$$

For UBe_{13}, the superconducting ground state develops before the T^2 behavior appears in the resistivity. By applying a magnetic field to quench the superconductivity, however, the T^2 behavior appears at low enough temperatures.[54] By extrapolating to zero field, a value of 120 $\mu\Omega$ cm/K^2 is estimated for the A coefficient of UBe_{13}. If the saturation resistivity is between 300 and 1000 $\mu\Omega$ cm, then the characteristic energy for UBe_{13} is between 2 and 5 cm^{-1}. This low-energy scale explains the difficulties encountered by Bonn *et al.*,[22] whose data extend to 15 cm^{-1}, much above the characteristic energy of the system. Perhaps, too, experiments should be done at lower temperatures for UBe_{13}, where the coherence of the HF state is well developed.

The FIR absorptivity of UPt_3 has been measured from 2 to 1000 cm^{-1} at 1.2 K. At very low frequencies the absorptivity is given by the classical skin effect with a scattering rate given by the dc resistivity. For higher frequencies the absorptivity rises to a value much higher than predicted from this dc scattering rate. To measure the absorptivity at very low frequencies, a highly sensitive transmission-line technique has been developed. Extending the data with recent data of Schoenes and Franse[34] and Marabelli *et al.*,[25] the conductivity over the whole frequency range is obtained from a Kramers-Kronig analysis. The behavior of the conductivity can be explained with a frequency-dependent scattering rate. Adopting a simple form for this scattering rate which describes the data leads to a large renormalization of the effective mass at frequencies less than 10 cm^{-1}. Using the quasiparticle self-energy obtained by Millis and Lee for the lattice Anderson model, the frequency-dependent scattering rate for low frequencies is calculated. The calculated results of Millis and Lee compare favorably with the experiment. Future studies of the absorptivity of HF systems must concentrate effort on the FIR frequency range and below, not the infrared or above.

ACKNOWLEDGMENTS

The authors have benefited from numerous conversations with J. W. Wilkins. The work at Cornell University was supported by National Science Foundation (NSF) Grant No. DMR-84-09823 and by the U.S. Army Research Office under Grant No. DAAL03-86-K-0103. One of us (P.E.S.) was partially supported by AT&T Bell Laboratories. Use of facilities supported by the Materials Science Center at Cornell University is acknowledged. Research at UCSD was supported by the U.S. Department of Energy under Grant No. DE-FG03-86ER45230. Work at Los Alamos National Laboratory (LANL) was carried out under the auspices of the U.S. Department of Energy, Office of Basic Energy Sciences, Division of Materials Science.

[1]G. R. Stewart, Rev. Mod. Phys. **56**, 755 (1984).
[2]T. Oguchi and A. J. Freeman, J. Magn. Magn. Mater. **52**, 174 (1985).
[3]R. C. Albers, A. M. Boring, and N. E. Christensen, Phys. Rev. B **33**, 8116 (1986).
[4]J. Sticht and J. Kubler, Solid State Commun. **54**, 389 (1985).
[5]P. Strange and B. L. Gyorffy, Physica B + C **130B**, 41 (1985).
[6]C. S. Wang, H. Krakauer, and W. E. Pickett, Physica B + C **135B**, 34 (1985).
[7]P. A. Lee, T. M. Rice, J. W. Serene, L. J. Sham, and J. W. Wilkins, Commun. Condens. Matter Phys. **12**, 99 (1986).
[8]S. L. Cooper, M. V. Klein, Z. Fisk, J. L. Smith, and H. R. Ott, Phys. Rev. B **35**, 2615 (1987).
[9]S. L. Cooper, R. T. Demers, M. V. Klein, Z. Fisk, and J. L. Smith, Physica B + C **135B**, 49 (1985).
[10]S. Horn, E. Holland-Moritz, M. Loewenhaupt, F. Steglich, H. Scheuer, A. Benoit, and J. Flouquet, Phys. Rev. B **23**, 3171 (1981).
[11]G. Aeppli, E. Bucher, and G. Shirane, Phys. Rev. B **32**, 7579 (1985).
[12]A. I. Goldman, S. M. Shapiro, G. Shirane, J. L. Smith, and Z. Fisk, Phys. Rev. B **33**, 1627 (1986).
[13]C. Stassis, B. Batlogg, J. P. Remeika, J. D. Axe, G. Shirane, and Y. J. Uemura, Phys. Rev. B **33**, 1680 (1986).
[14]C. Stassis, J. Arthur, C. Majkrzak, J. Axe, B. Batlogg, J. Remeika, Z. Fisk, J. L. Smith, and A. Edelstein, Phys. Rev. B **34**, 4382 (1986).
[15]M. Moser, P. Wachter, and J. J. M. Franse, Solid State Commun. **58**, 515 (1986).
[16]*Theory of Heavy Fermions and Valence Fluctuators*, edited by

T. Kasuya and T. Saso (Springer-Verlag, Berlin, 1985).
[17]F. E. Pinkerton, B. C. Webb, A. J. Sievers, J. W. Wilkins, and L. J. Sham, Phys. Rev. B **30**, 3068 (1984).
[18]B. C. Webb, A. J. Sievers, and T. Mihalisin, Phys. Rev. Lett. **57**, 1951 (1986).
[19]A. de Visser, J. J. M. Franse, and A. Menovsky, J. Magn. Magn. Mater. **43**, 43 (1984).
[20]D. Jaccard, J. Flouquet, P. Lejay, and J. L. Tholence, J. Appl. Phys. **57**, 3082 (1985).
[21]K. Kadowaki, A. Umezawa, and S. B. Woods, J. Magn. Magn. Mater. **54-57**, 385 (1986).
[22]D. A. Bonn, R. J. Klassen, T. Timusk, J. L. Smith, and Z. Fisk (unpublished).
[23]S. A. Oliver, S. W. McKnight, A. L. Giorgi, and G. R. Stewart, Bull. Am. Phys. Soc. **31**, 343 (1986).
[24]G. A. Thomas, H. K. Ng, and E. Bucher, Bull. Am. Phys. Soc. **31**, 344 (1986).
[25]F. Marabelli, G. Travaglini, P. Wachter, and J. J. M. Franse, Solid State Commun. **59**, 381 (1986).
[26]F. Wooten, *Optical Properties of Solids* (Academic, New York, 1972).
[27]A. J. Millis and P. A. Lee, Phys. Rev. B **35**, 3394 (1987).
[28]F. E. Pinkerton, Inf. Phys. **22**, 337 (1982).
[29]B. C. Webb, A. J. Sievers, and T. Mihalisin, J. Appl. Phys. **57**, 3134 (1985).
[30]G. Brändli and A. J. Sievers, Phys. Rev. B **5**, 3550 (1972).
[31]N. Marcuvitz, *Waveguide Handbook* (McGraw-Hill, New York, 1951).
[32]B. C. Webb, Ph.D. thesis, Cornell University, 1985, available from University Microfilms, Ann Arbor, MI.
[33]J. J. M. Franse, A. Menovsky, A. de Visser, C. D. Bredl, U. Gottwick, W. Lieke, H. M. Mayer, U. Rauchschwalbe, G. Sparn, and F. Steglich, Z. Phys. B **59**, 15 (1985).
[34]J. Schoenes and J. J. M. Franse, Physica B + C **130B**, 69 (1985).
[35]N. V. Smith, Phys. Rev. B **9**, 1365 (1975).
[36]A. de Visser, J. J. M. Franse, A. Menovsky, and T. T. M. Palstra, Physica B + C **127B**, 442 (1984).
[37]N. W. Ashcroft and N. D. Mermin, *Solid State Physics* (Holt, Rinehart, and Winston, New York, 1975).
[38]J. W. Chen, S. E. Lambert, M. B. Maple, Z. Fisk, J. L. Smith, G. R. Stewart, and J. O. Willis, Phys. Rev. B **30**, 1583 (1984).
[39]J. Schoenes and J. J. M. Franse, Phys. Rev. B **33**, 5138 (1986).
[40]J. M. Ziman, *Electrons and Phonons: The Theory of Transport Phenomena in Solids* (Oxford University Press, London, 1960).
[41]A. de Visser, J. M. M. Franse, and A. Menovsky, J. Phys. F **15**, L53 (1985).
[42]P. H. Frings and J. M. M. Franse, Phys. Rev. B **31**, 4355 (1985).
[43]W. R. Datars, K. Kadowaki, N. Ali, and S. B. Woods, J. Phys. F **16**, L63 (1986).
[44]J. J. M. Franse, A. de Visser, A. Menovsky, and P. H. Frings, J. Magn. Magn. Mater. **52**, 61 (1985).
[45]V. Muller, D. Maurer, K. de Groot, E. Bucher, and H. E. Bommel, Phys. Rev. Lett. **56**, 248 (1986).
[46]J. W. Wilkins (private communication).
[47]J. Serene and J. W. Wilkins, Bull. Am. Phys. Soc. **32**, 720 (1987).
[48]A. A. Abrikosov, L. P. Gor'kov, and I. Ye. Dzyaloshinskii, *Quantum Field Theoretical Methods in Statistical Physics* (Pergamon, New York, 1965).
[49]K. K. Murata, Ph.D. thesis, Cornell University, 1971.
[50]P. B. Allen, Phys. Rev. B **3**, 305 (1971).
[51]R. N. Gurzhi, Zh. Eksp. Teor. Fiz. **35**, 965 (1958) [Sov. Phys.—JETP **8**, 673 (1959)].
[52]P. S. Riseborough, Phys. Rev. B **27**, 5775 (1983).
[53]J. R. Thompson, J. Appl. Phys. **53**, 7894 (1982).
[54]G. Remenyi, D. Jaccard, J. Flouquet, A. Briggs, Z. Fisk, J. L. Smith, and H. R. Ott, J. Phys. (France) **47**, 367 (1986).